This is the Pre-Published Version.

https://doi.org/10.1016/j.ceramint.2021.03.243

Spraying fabrication of spectrally selective coating with improved near-infrared shielding performance for energy-efficient glazing

Boxu Shen[1], Yuanhao Wang[2,*], Lin Lu[1], Hongxing Yang[1,*]

1. Renewable Energy Research Group (RERG), Department of Building Services Engineering, The Hong Kong Polytechnic University, Kowloon, Hong Kong

2. SUSTech Engineering Innovation Center, School of Environmental Science and Engineering, Southern University of Science and Technology, Shenzhen, Guangdong 518055, China

*Corresponding author: Yuanhao Wang; Hongxing Yang

E-mail addresses: yuanhaowang@yahoo.com, wangyh2020@mail.sustech.edu.cn (Y. Wang);

hong-xing.yang@polyu.edu.hk (H. Yang)

Tel./Fax numbers: +86 13826520347 (Y. Wang); +852 2766-5863 (H. Yang)

Abstract

In this study, spectrally selective coating with improved near-infrared shielding property was fabricated by direct spray technique using the $Cs_{0.33}WO_3$ and Sb-doped SnO_2 as composite filler. The effect of Cs/W molar ratio on phase composition, crystal structure, morphology, chemical state and optical property was investigated. The results reveal that the Cs/W molar ratio has a significant influence in promoting the form of hexagonal crystal structure, which is beneficial to improve spectral selectivity. Especially, when the Cs/W molar ratio was 0.375, the as-synthesized $Cs_{0.33}WO_3$ product demonstrated the desired phase composition and W^{5+} generation. Furthermore, the spectrally selective coating prepared by the dispersion with 10 wt% composite filler combined with $Cs_{0.33}WO_3$ and Sb-doped SnO_2 presented optimal optical performance. The excellent near-infrared shielding performance of the spectrally selective coating indicates great potential in the field of energy-efficient glazing.

Keywords: $Cs_{0.33}WO_3$, Sb-doped SnO_2, near-infrared shielding, spray fabrication, spectrally

selective coating, energy-efficient glazing

1. Introduction

Glazing materials are increasingly used as an important component in modern construction industry for aesthetics and daylight. Generally, the glazing used for windows refers to soda-lime glass which is made of silica, sodium oxide, lime and a small quantity of other additives via floating process. The transmittance of clear soda-lime glass for visible and near-infrared light is about 75 % to 90 % at 4 mm thickness, indicating that the glazing lacks the spectrally selective property [1]. Accordingly, strong radiation can increase the indoor temperature in buildings, which leads to the increase of air-conditioning power consumption especially for regions with cooling-demand climate [2, 3]. Therefore, suitable spectrally selective materials applied in the field of glazing functionalization are desired for energy-saving.

Glass functionalization is usually realized by a thin film layer based on spectrally selective materials applied on the glazing surface thus changing the way the glass interacting with the solar radiation and surrounding media. So far, the spectrally selective materials can be classified into three main types, namely metal, metal oxides and metalloid. The most commonly used metal for spectral selectivity is silver. Silver-based low-emissivity (low-E) glazing is composed of two glass panes for preventing the exposure of the low-E coating which is usually fabricated by magnetron sputtering requiring expensive equipment and complex operating parameters [4, 5]. This type energy-saving glass is not favorable for retrofitting the installed single-glazed windows due to its double structure. Metal oxides used for solar heat-shielding mainly include tin-doped indium oxide (ITO) [6-8], aluminum-doped zinc oxide (AZO) [9-11] and Sb-doped tin oxide (ATO) [12-16]. Among them, ITO and ATO can only block the wavelength higher than 1500nm, which

might cause a lower shielding performance in the wavelength ranging from 780nm to 1500nm [17]. Also, the raw material (indium) for preparing ITO is expensive. It is reported that the method for preparing AZO is not efficient and it shows a higher transmittance in the near-infrared region [18]. As for metalloid, LaB_6, the most common rare-earth hexaborides, can effectively shield the near-infrared radiation. However, its high hardness restricts the large-scale production for commercialization [19]. By contrast, it is reported that hexagonal cesium tungsten bronze (Cs-HTB) nanoparticles display great near-infrared shielding property in the wavelength ranging from 800nm to 1500nm, indicating that the solar heat-shielding property is not good enough in the wavelength larger than 1500nm [20-22]. Although some cheap raw materials have been used to synthesize the Cs-HTB nanoparticles, it still requires a subsequent thermal treatment in H_2/N_2 atmosphere. It was reported that the thermal treatment could lead to the secondary growth of the nanocrystals causing an increase of nanoparticle size, which is detrimental to the visible transmittance of the final coating [23]. Furthermore, the spectrally selective coating based on the nanoparticles are usually prepared via spinning and rolling method [24-26]. However, spinning coating is a lab-scale method and rolling coating is not conductive to obtain an even coating surface. Simple and accessible deposition methods are important not only for academic study but also for industrial use.

Herein, we propose a facile spraying method to prepare spectrally selective coating combined with ATO and Cs-HTB nanoparticles for improved energy-saving glazing. Low-agglomerated ATO nanoparticles were prepared based on our previous research [13]. Cs-HTB nanoparticles were prepared using one step solvothermal method without subsequent thermal treatment using tungsten hexachloride as W source. The effect of Cs/W ratio on the microstructure, morphology,

phase composition and near-infrared blocking property were investigated. The spectrally selective coating fabricated using as-prepared nanoparticles exhibited improved solar heat-shielding performance in the whole near-infrared spectral range. Especially, when the Cs/W molar ratio was 0.375, the solar heat-shielding performance of Cs-HTB nanoparticles was obviously improved. The results play an important reference value for developing spectrally selective coatings, and the synthesized Cs-HTB nanoparticles shows typically hexagonal crystal structure without additional heat treatment. It is believed that the spraying fabrication of spectrally selective coating with improved near-infrared shielding performance has promising applied prospects for energy-efficient glazing.

2. Experimental

2.1 Materials

Tungsten hexachloride (WCl_6), cesium hydroxide monohydrate ($CsOH·H_2O$), absolute ethanol, acetic acid (CH_3COOH), antimony chloride ($SbCl_3$, AR), deionized water, polyvinyl alcohol (PVA), tin chloride pentahydrate ($SnCl_4·5H_2O$, AR), ammonia water ($NH_3·H_2O$, AR), and waterborne polyurethane were obtained by Aladdin Chemistry Co., Ltd. The chemicals purchased were used without further purification.

2.2 Preparation of Cs-HTB nanoparticles and ATO nanoparticles

Firstly, a specific amount of tungsten hexachloride was dissolved in the absolute ethanol with fast stirring, then cesium hydroxide monohydrate was added into the WCl_6 ethanol precursor to obtain homogeneous solution. The molar ratio of Cs/W was formulated as 0.125, 0.250, 0.375, 0.500 respectively. The concentration of WCl_6 was 0.1 mol/L. After that, acetic acid was added, then the whole solution was transferred into a 200 ml Teflon-lined autoclave, followed by

solvothermal reaction at 220 ℃ for 24 h. The as-prepared blue powder was rinsed with ethanol 3 times and dried in a vacuum oven at 60 ℃ overnight. The ATO nanoparticles were prepared using a reported co-precipitation method [13].

2.3 Spraying fabrication of spectrally selective coatings on glazing

The PVA water solution with the mass concentration of 5 wt% acted as the film-forming agent, then BYK dispersant was introduced into the solution as stable agent for preventing the agglomeration in nanoparticles. Certain amount of as-synthesized Cs-HTB and ATO nanoparticles were added into the above solution with 1:1 mass ratio of Cs-HTB and ATO. The obtained dispersion was then processed by ultrasonic treatment. Finally, the coating solution was used to fabricate the spectrally selective coating on the clear glass by spray method.

2.4 Characterization

The phase compositions of nanoparticles were examined by X-ray diffraction (XRD) with Cu Kα radiation. The morphologies and microstructures of the nanoparticles were obtained by transmission electron microscopy (TEM) with an energy dispersive spectrum (EDS) attachment. The chemical composition and binding energies of W 4f were obtained by X-ray photoelectron spectroscopy (XPS). The optical performance of the prepared samples was measured by an UV-vis-NIR spectrophotometer.

2.5 Near-infrared shielding test

A box device was conducted to assess the heat-shielding property of the different glazing samples. Fig. 7a displays the diagram of the test device. The top facet of device was equipped with the different glazing. The light was provided by a 500 W infrared lamp with 20 cm over the coated glass. The thermocouple should avoid being directly irradiated by the infrared lamp. The

temperature recorded by thermocouple represented the air temperature inside the sealed box device.

3. Results and discussion

XRD analysis was applied to investigate the phase composition and crystal structure of as-synthesized samples [27]. Fig. 1 presents XRD patterns of powder samples with Cs/W molar ratio of 0.125, 0.250, 0.375 and 0.500. The XRD patterns of Cs/W = 0.125 and 0.250 are indexed to a mixed crystal phase of the orthorhombic phase (JCPDS 74-2207) and hexagonal phase (JCPDS 83-1334). The results indicate that there are no obvious XRD peaks of monoclinic phase (JCPDS 36-0103). When the molar ratio was increased to 0.375, a pure hexagonal crystal phase appeared without evident miscellaneous peaks, which has been proved that hexagonal tungsten bronze exhibits superior near-infrared shielding performance due to high concentration of free carriers. As for the sample with Cs/W molar ratio of 0.500, it can be seen that cubic phase Cs_2WO_6 (JCPDS 81-1259) appeared besides hexagonal phase. It can be observed that with the increase of Cs/W molar ratio, the diffraction peak of (200) plane slightly shifted to a smaller angle, which can be illustrated by the Bragg equation. The decrease of angle indicates the larger lattice spacing. The diffraction peaks were broad when the Cs/W molar ratio was 0.125 and became more intense with the increase of molar ratio, indicating higher crystallinity of the as-synthesized samples. When the ratio was 0.500, the high dopant concentration caused the emergence of the cubic phase, which is not conducive to its near-infrared shielding property. In addition, it is obvious that breadth at half-maximum height of the main diffraction peaks was relatively wide, which is in accordance with the general characteristics of nanoparticles. Inspired by this, the average crystallite size (D) of Cs-HTB nanoparticles synthesized with different Cs/W molar ratio

was calculated by full line width at half maximum height (FWHM) of diffraction peaks via Scherrer formula and the results are presented in Table 1.

The TEM images of the as-synthesized samples with different Cs/W molar ratio are presented in Fig. 2. It is obvious that the Cs/W molar ratio significantly influences the morphology of the samples. When the Cs/W ratio was low, the as-synthesized sample shown in Fig. 2a tended to form agglomerated clusters composed of rod-like particles. When the doping molar ratio increased to 0.250, the irregular agglomerates consisting of the slender rod-like particles with a diameter of 20 nm to 50 nm could be obviously seen in the Fig. 2b. By increasing the ratio to 0.375 (Fig. 2c), it is found that the size of the agglomerates declined and the aspect ratio of the rod-like particles was reduced. A certain amount of small grains was randomly attached on the large grain surface of the sample with Cs/W molar ratio of 0.500. The small grains on the large grains caused an increase of the overall particle size, which is not favorable for localized surface plasmon resonance [28, 29].

More detailed structural information was determined using transmission electron microscopy (TEM). Fig. 3 presents the TEM image, HR-TEM image, SAED pattern and EDS pattern of the as-synthesized sample with the Cs/W molar ratio of 0.375. In Fig. 3a, most of prepared nanoparticles show a rectangle shape. Fig. 3b is the HR-TEM image of selected area in Fig. 3a and the lattice spacing is 0.3341 nm and 0.2739 nm, which is determined as plane of (111) and (112) respectively. The as-synthesized sample with the molar ratio of 0.375 with hexagonal crystal structure is confirmed by the SAED pattern displayed in Fig. 3c. The element composition is shown in Fig. 3d, indicating the existence of Cs, W and O element. Besides, the measured Cs/W molar ratio is about 0.301 which is quite close to that of the desired hexagonal $Cs_{0.33}WO_3$

nanoparticles.

The surface elements of the as-synthesized sample were investigated by XPS analysis. Fig. 4 presents the XPS spectra of the obtained sample with the Cs/W molar ratio of 0.375. As shown in Fig. 4a, the full-range XPS spectrum further confirms the existence of Cs, W and O elements and no other elements could be observed except for carbon. The W 4f core-level spectrum shown in Fig. 4b can be fitted as two spin-orbit doublets with a separation interval of 2.1 eV. The binding energy peaks at 38.1 eV and 36.0 eV can be ascribed to W^{6+} [25, 30]. The presence of W^{5+} is confirmed by the peaks with binding energy of 36.7 eV and 34.6 eV. The results conformed well with the values reported in previous works. It can be obtained that the Cs-HTB nanoparticles with the Cs/W molar ratio of 0.375 contain a reduced chemical state of W^{5+} besides W^{6+}.

The synthesis of antimony doped tin oxide (ATO) was carried out using the method proposed by a previous work [13]. Fig. 5a presents the diffraction peaks are well indexed to the standard pattern, indicating that the ATO nanoparticles were successfully prepared. Fig. 5b illustrates the SAED pattern of the inset area, further demonstrating the desired crystal structure. In Fig 5c, the survey XPS spectrum clearly presents the existence of Sn, Sb and O element. The binding energies of doublets were reported as 487 eV and 496 eV, respectively, which is ascribed to the existence of Sn 3d [31, 32]. Fig. 5d displays the core-level XPS spectrum of Sb 3d doublets. The binding energies of the Sb 3d were reported in the scope of 525-545 eV. It is found that antimony can be doped in the crystal structure with two oxidation valences, namely Sb^{5+} and Sb^{3+}.

To fabricate the spectrally selective coatings, the as-synthesized ATO and Cs-HTB nanoparticles with Cs/w molar ratio of 0.375 were combined with the same mass ratio as the composite nanofiller. Fig. 6 presents the solar transmittance spectra of the coated glazing prepared

by the dispersion with different nanofiller content of 6 wt%, 8 wt%, 10 wt% and 12 wt%. For the purpose of evaluating the optical properties of the coatings, three parameters, including T_{Vis} (average transmittance of visible light, 380-780 nm), T_{NIR} (average transmittance of near-infrared light, 780-2500 nm) and K (transparent heat-shieling index defined as $K = T_{Vis} / T_{NIR}$), were proposed [33, 34]. The corresponding values calculated by the fitting curve of transmittance spectra shown in Fig. 6 are displayed in Table 2. It can be seen that the solid content of composite nanofiller plays a major role on improving the near-infrared blocking property. In general, higher K indicates better transparent heat-shielding performance of the coatings. As shown in Table 2, T_{NIR} declines with the increase of solid content, indicating higher near-infrared shielding ability. Although K is higher with the increase of solid content, T_{Vis} shows a decreasing trend. When the solid content attains to 12 wt%, T_{Vis} of the corresponding coating is below 70%, which is not conducive to visible transmittance. Therefore, a conclusion can be drawn that the spectrally selective coating with the solid content of 10 wt% displayed favorable transparent heat-shielding performance than the coatings with other solid contents.

The near-infrared blocking property of the glass with as-prepared spectrally selective coating, ITO glass and ordinary glass was investigated by a simulated test using a 250 W halogen lamp as infrared source. The test device is shown in the Fig. 7a, in which the temperature measured by thermocouple indicates the air temperature inside the sealed box. It can be seen that the top side of the device is composed of two glasses with a hollow structure and the sample glass pending test was placed under the ordinary glass. The reason for this design is to minimize the influence of non-radiative heat transfer. As shown in Fig. 7b, the schematic of transparent heat-shielding mechanism is presented, which is ascribed to its superior spectral selectivity. Fig. 7c shows the

UV-Vis-NIR transmittance spectra of coated glass, ITO glass and ordinary glass. It can be seen that the coated glass showed lower transmittance in the near-infrared wavelength range and maintain a relatively high visible transparency. Fig. 7d presents the temperature variation recorded by thermocouple of the three glazing samples with the irradiation time. It is observed that the measured temperature with coated glass demonstrated slowest heating rate. The temperature gap between the coated glass and ordinary glass reaches 6.5℃ under 1 h radiation, indicating that the spectrally selective coating on the glass is of excellent near-infrared shielding property. The coated glass is expected to reduce the cooling loads of air-conditioning in summer, aiming to realize energy-saving and emission reduction. By contrast, the ITO glass shows worse near-infrared shielding performance than the coated glass, which only decreases the measured temperature by 2.8℃ compared with ordinary glass. Consequently, the coated glass demonstrates better spectral selectivity than the ITO glass, and it can be expected that the spectrally selective coating with high visible transmittance and near-infrared shielding property can promote the practical applications in the field of energy-efficient glazing.

4. Conclusions

In this work, spectrally selective coating with improved near-infrared shielding property was successfully fabricated by simple spraying technique. It is found that the phase composition and morphology of the Cs-HTB nanoparticles were significantly influenced by the Cs/W molar ratio. When the Cs/W molar ratio attained 0.375, the hexagonal tunnel was formed to access more Cs^{+} ions in the crystal structure, which is beneficial for LSPR response. Besides, the Cs doping is favorable for the formation of W^{5+}, which is the evident of the high concentration of free electrons. The composite filler combined with Cs-HTB and ATO improved the near-infrared blocking

property of the spectrally selective coating. It is proved that the coating prepared the dispersion with solid content of 10 wt% for energy-efficient glazing was of visible T_{Vis} of 70.76%, T_{NIR} of 9.36% and K of 7.56. Furthermore, a directly simple spray fabrication of the spectrally selective coating with improved near-infrared shielding performance is of a positive impact to promote the practical application of the energy-efficient glazing.

Declaration of competing interest

The authors declare that they have no known competing financial interests or personal relationships that could have appeared to influence the work reported in this paper.

Acknowledgements

This work was supported by the TCS project of the Hong Kong Innovation and Technology Fund (UIT/139) and Sola Green Technologies Limited.

References

[1] Ke Y, Chen J, Lin G, Wang S, Zhou Y, Yin J, et al. Smart Windows: Electro- , Thermo- , Mechano- , Photochromics, and Beyond. Advanced Energy Materials. 2019;9.

[2] Ghosh A, Norton B. Advances in switchable and highly insulating autonomous (self-powered) glazing systems for adaptive low energy buildings. Renewable Energy. 2018;126:1003-31.

[3] Rezaei SD, Shannigrahi S, Ramakrishna S. A review of conventional, advanced, and smart glazing technologies and materials for improving indoor environment. Solar Energy Materials and Solar Cells. 2017;159:26-51.

[4] Abundiz-Cisneros N, Sanginés R, Rodríguez-López R, Peralta-Arriola M, Cruz J, Machorro R. Novel Low-E filter for architectural glass pane. Energy and Buildings. 2020;206.

[5] Ye X, Wang Z, Zhang L, Wang Q, Xiao X, Cai S, et al. Synthesis and infrared emissivity properties

of novel polyurethane/Ag/ZnO array composite coatings. Infrared Physics & Technology. 2019;102.

[6] Swallow JEN, Williamson BAD, Sathasivam S, Birkett M, Featherstone TJ, Murgatroyd PAE, et al. Resonant doping for high mobility transparent conductors: the case of Mo-doped In2O3. Materials Horizons. 2020;7:236-43.

[7] Maho A, Comeron Lamela L, Henrist C, Henrard L, Tizei LHG, Kociak M, et al. Solvothermally-synthesized tin-doped indium oxide plasmonic nanocrystals spray-deposited onto glass as near-infrared electrochromic films. Solar Energy Materials and Solar Cells. 2019;200.

[8] Liu H, Zeng X, Kong X, Bian S, Chen J. A simple two-step method to fabricate highly transparent ITO/polymer nanocomposite films. Applied Surface Science. 2012;258:8564-9.

[9] Jiang S, Xu J, Miao D, Peng L, Shang S, Zhu P. Water-repellency, ultraviolet protection and infrared emissivity properties of AZO film on polyester fabric. Ceramics International. 2017;43:2424-30.

[10] Jelle BP, Kalnæs SE, Gao T. Low-emissivity materials for building applications: A state-of-the-art review and future research perspectives. Energy and Buildings. 2015;96:329-56.

[11] Hamza MK, Bluet JM, Masenelli-Varlot K, Canut B, Boisron O, Melinon P, et al. Tunable mid IR plasmon in GZO nanocrystals. Nanoscale. 2015;7:12030-7.

[12] Wang M, Xu Y, Liu Y, Wu W, Xu S. Synthesis of Sb-doped SnO2 (ATO) hollow microspheres and its application in photo-thermal shielding coating. Progress in Organic Coatings. 2019;136.

[13] Shen B, Wang Y, Lu L, Yang H. Synthesis and characterization of Sb-doped SnO2 with high near-infrared shielding property for energy-efficient windows by a facile dual-titration co-precipitation method. Ceramics International. 2020;46:18518-25.

[14] Yang L, Huang J, Shi L, Cao L, Liu H, Liu Y, et al. Sb doped SnO2-decorated porous g-C3N4 nanosheet heterostructures with enhanced photocatalytic activities under visible light irradiation.

Applied Catalysis B: Environmental. 2018;221:670-80.

[15] Wu K, Xiang S, Zhi W, Bian R, Wang C, Cai D. Preparation and characterization of UV curable waterborne poly(urethane-acrylate)/antimony doped tin oxide thermal insulation coatings by sol-gel process. Progress in Organic Coatings. 2017;113:39-46.

[16] Wang X, Hu Y, Song L, Xing W, Lu H, Lv P, et al. Effect of antimony doped tin oxide on behaviors of waterborne polyurethane acrylate nanocomposite coatings. Surface and Coatings Technology. 2010;205:1864-9.

[17] Xu X, Zhang W, Hu Y, Wang Y, Lu L, Wang S. Preparation and overall energy performance assessment of wide waveband two-component transparent NIR shielding coatings. Solar Energy Materials and Solar Cells. 2017;168:119-29.

[18] Zhang W, Jiang S, Lv D. Fabrication and characterization of a PDMS modified polyurethane/Al composite coating with super-hydrophobicity and low infrared emissivity. Progress in Organic Coatings. 2020;143.

[19] Zheng L, Xiong T, Shah KW. Transparent nanomaterial-based solar cool coatings: Synthesis, morphologies and applications. Solar Energy. 2019;193:837-58.

[20] Liu G, Kong F, Xu J, Li R. Novel synthesis of 0D, 1D and 2D nano-CsxWO3 and their tunable optical-thermal response performance. Journal of Materials Chemistry C. 2020.

[21] Ran S, Liu J, Shi F, Fan C, Yang J, Chen B, et al. Microstructure regulation of CsxWO3 nanoparticles by organic acid for improved transparent thermal insulation performance. Materials Research Bulletin. 2019;109:273-80.

[22] Liu J, Ran S, Fan C, Qiao Y, Shi F, Yang J, et al. One pot synthesis of Pt-doped CsxWO3 with improved near infrared shielding for energy-saving film applications. Solar Energy. 2019;178:17-24.

[23] Zhou Y, Li N, Xin Y, Cao X, Ji S, Jin P. CsxWO3 nanoparticle-based organic polymer transparent foils: low haze, high near infrared-shielding ability and excellent photochromic stability. Journal of Materials Chemistry C. 2017;5:6251-8.

[24] Wang Q, Li C, Xu W, Zhao X, Zhu J, Jiang H, et al. Effects of Mo-doping on microstructure and near-infrared shielding performance of hydrothermally prepared tungsten bronzes. Applied Surface Science. 2017;399:41-7.

[25] Yao Y, Zhang L, Chen Z, Cao C, Gao Y, Luo H. Synthesis of Cs x WO 3 nanoparticles and their NIR shielding properties. Ceramics International. 2018;44:13469-75.

[26] Ran S, Liu J, Shi F, Fan C, Chen B, Zhang H, et al. Greatly improved heat-shielding performance of KxWO3 by trace Pt doping for energy-saving window glass applications. Solar Energy Materials and Solar Cells. 2018;174:342-50.

[27] Tahmasebi N, Madmoli S, Farahnak P. Synthesis of cesium tungsten bronze nanofibers with different crystalline phases. Materials Letters. 2018;211:161-4.

[28] Staller CM, Gibbs SL, Saez Cabezas CA, Milliron DJ. Quantitative Analysis of Extinction Coefficients of Tin-Doped Indium Oxide Nanocrystal Ensembles. Nano Lett. 2019;19:8149-54.

[29] Guo C, Yin S, Yan M, Sato T. Facile synthesis of homogeneous CsxWO3 nanorods with excellent low-emissivity and NIR shielding property by a water controlled-release process. Journal of Materials Chemistry. 2011;21.

[30] Song X, Liu J, Shi F, Fan C, Ran S, Zhang H, et al. Facile fabrication of KmCsnWO3 with greatly improved near-infrared shielding efficiency based on W5+-induced small polaron and local surface plasmon resonance (LSPR) modulation. Solar Energy Materials and Solar Cells. 2020;218.

[31] Hu Y, Zhong H, Wang Y, Lu L, Yang H. TiO2/antimony-doped tin oxide: Highly water-dispersed

nano composites with excellent IR insulation and super-hydrophilic property. Solar Energy Materials and Solar Cells. 2018;174:499-508.

[32] Li Y, Zeng G, Yang G, Wu Q, Zhang H, Li W, et al. Synthesis, characterization and properties of ATO/potassium silicate film prepared by twice spray pyrolysis. Journal of Alloys and Compounds. 2019;772:240-6.

[33] Cai L, Wu X, Gao Q, Fan Y. Effect of morphology on the near infrared shielding property and thermal performance of K0.3WO3 blue pigments for smart window applications. Dyes and Pigments. 2018;156:33-8.

[34] Zhao Z, Bai Y, Ning W, Fan J, Gu Z, Chang H, et al. Effect of surfactants on the performance of 3D morphology W18O49 by solvothermal synthesis. Applied Surface Science. 2019;471:537-44.

Table 1

Table 1

The calculated crystallite size using the Scherrer formula.

Cs/W molar ratio	0.125	0.250	0.375	0.500
D/nm	16.15	12.55	14.30	12.80

Table 2

Table 2

The optical parameters of the spectrally selective coatings with different solid content of composite nanofillers.

Solid content	T_{Vis} (%)	T_{NIR} (%)	K
6 wt%	76.31%	19.11%	6.03
8 wt%	71.65%	11.06%	6.47
10 wt%	70.76%	9.36%	7.56
12 wt%	68.81%	7.55%	9.11

Figure 1

Click here to download Figure: Fig. 1.docx

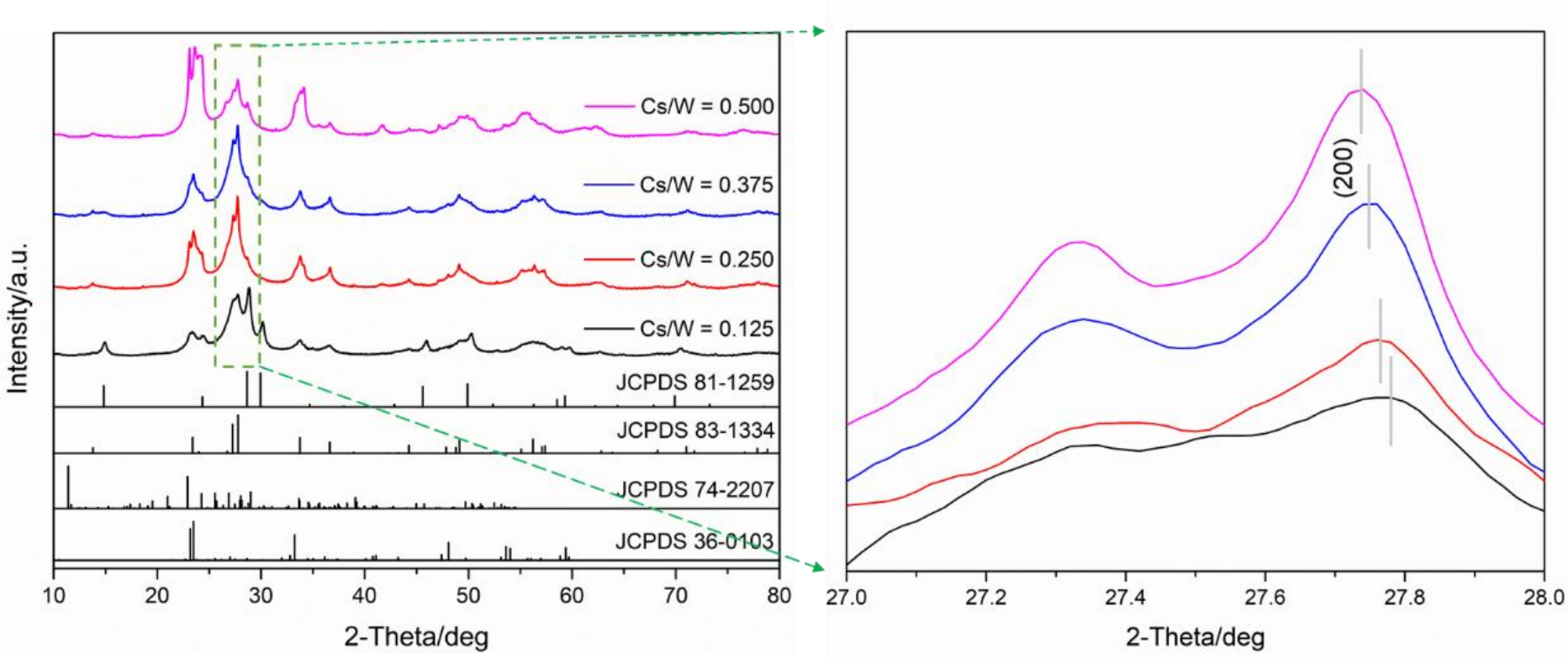

Fig. 1 XRD patterns of as-synthesized samples with the Cs/W molar ratio of 0.125, 0.250, 0.375, 0.500)

Figure 2

Click here to download Figure: Fig. 2.docx

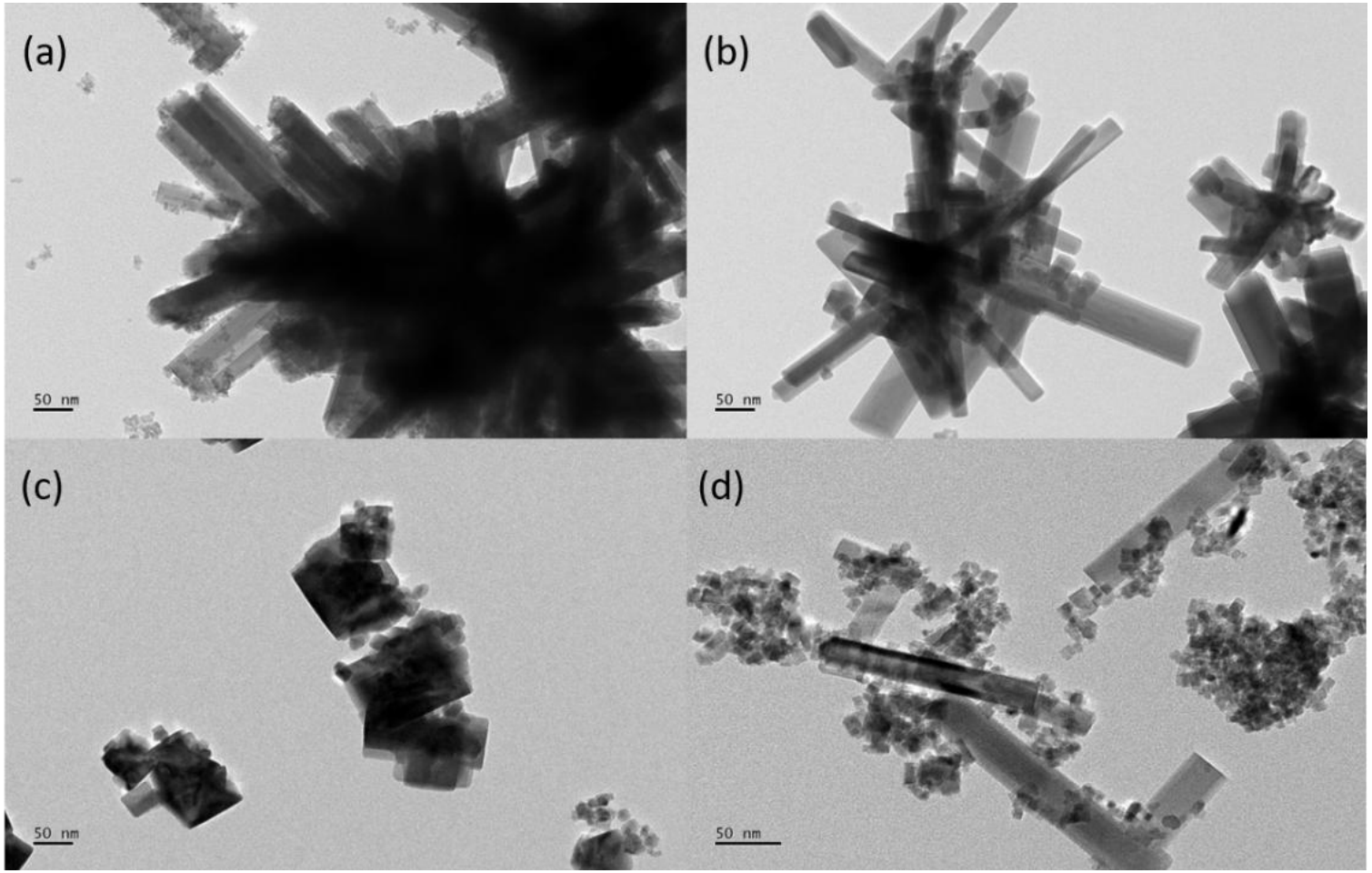

Fig. 2 TEM images of as-prepared samples with different Cs/W molar ratio of (a) 0.125, (b) 0.250, (c) 0.375 and (d) 0.500

Figure 3

Click here to download Figure: Fig. 3.docx

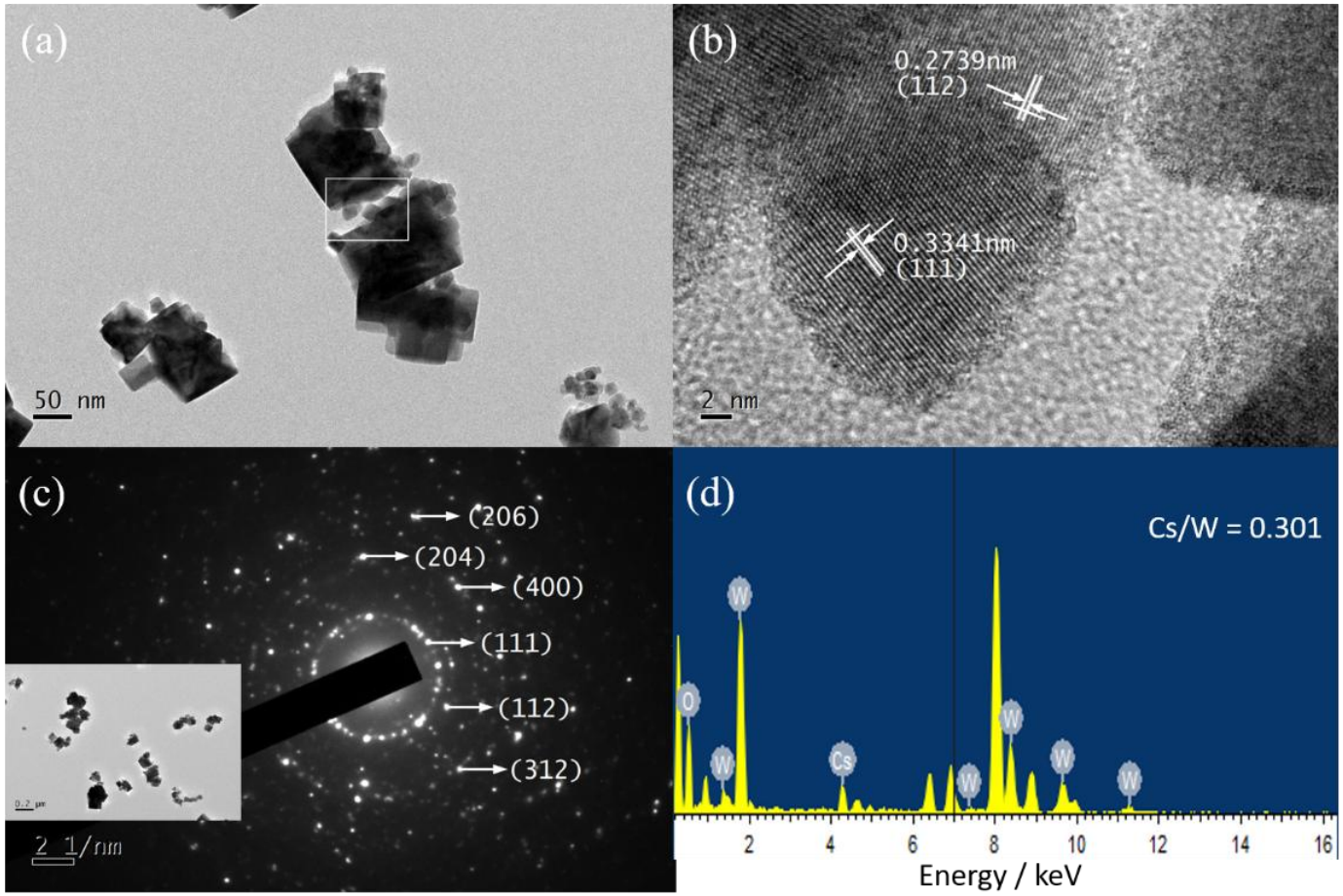

Fig. 3 (a) TEM image of as-prepared sample with the Cs/W molar ratio of 0.375, (b) HR-TEM image of selected area, (c) SAED pattern of inset area and (d) EDS pattern of the sample with a nominal Cs/W molar ratio of 0.375

Figure 4

Click here to download Figure: Fig. 4.docx

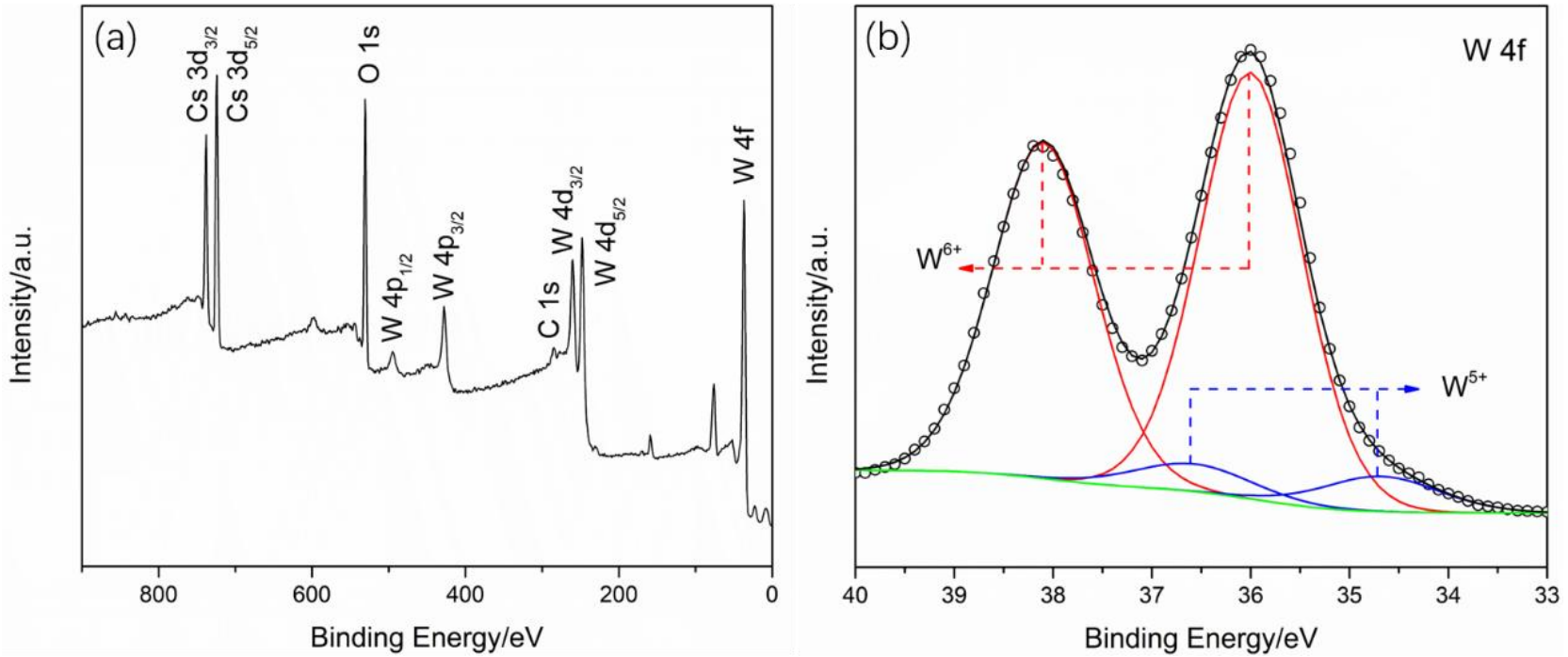

Fig. 4 (a) Survey XPS spectrum and (b) W 4f core-level XPS spectrum of the prepared sample with the Cs/W molar ratio of 0.375

Figure 5

Click here to download Figure: Fig. 5.docx

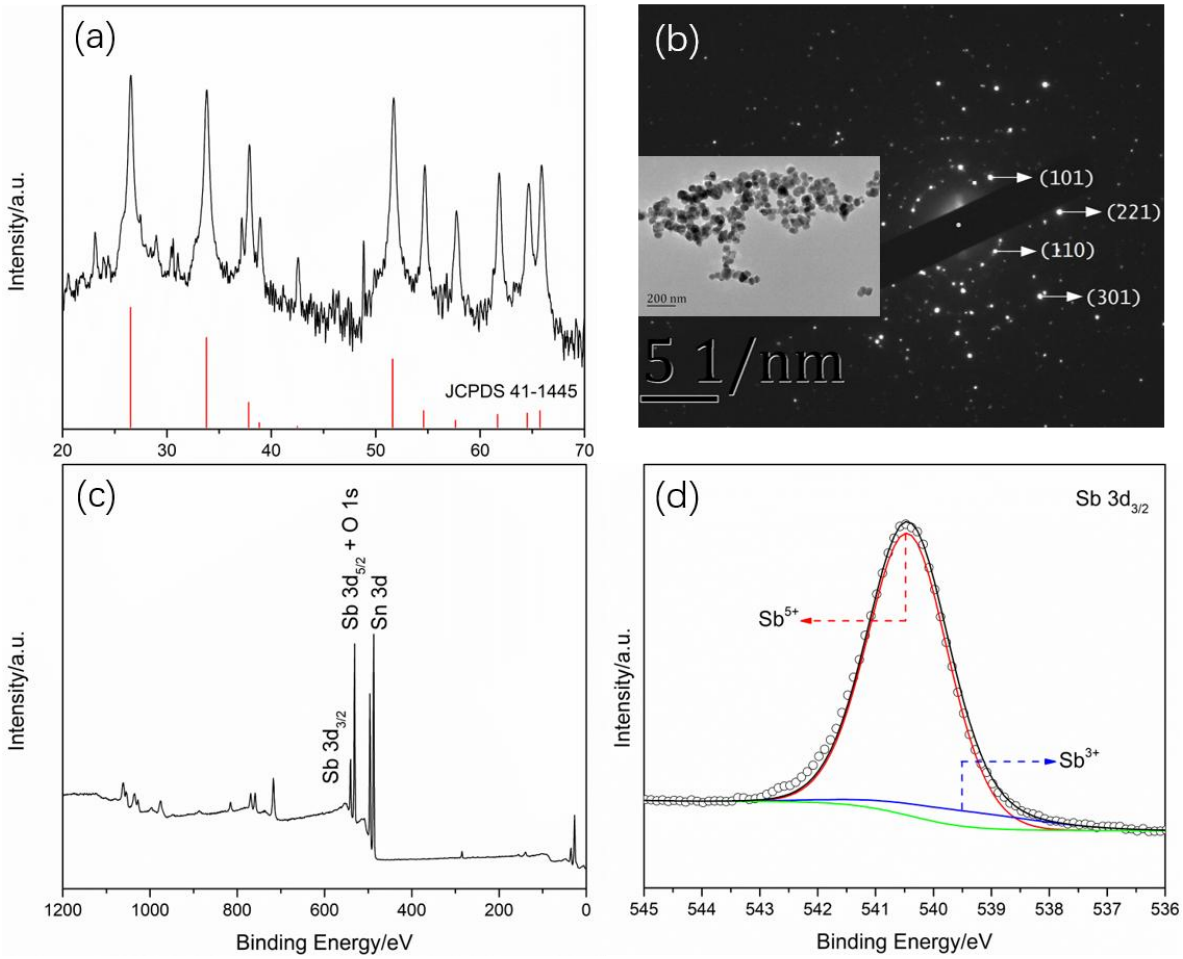

Fig. 5 (a) XRD pattern, (b) SAED pattern of inset area, (c) full-range XPS spectrum and (d) Sb 3d core-level XPS spectrum of the as-prepared ATO nanoparticles.

Figure 6

Click here to download Figure: Fig. 6.docx

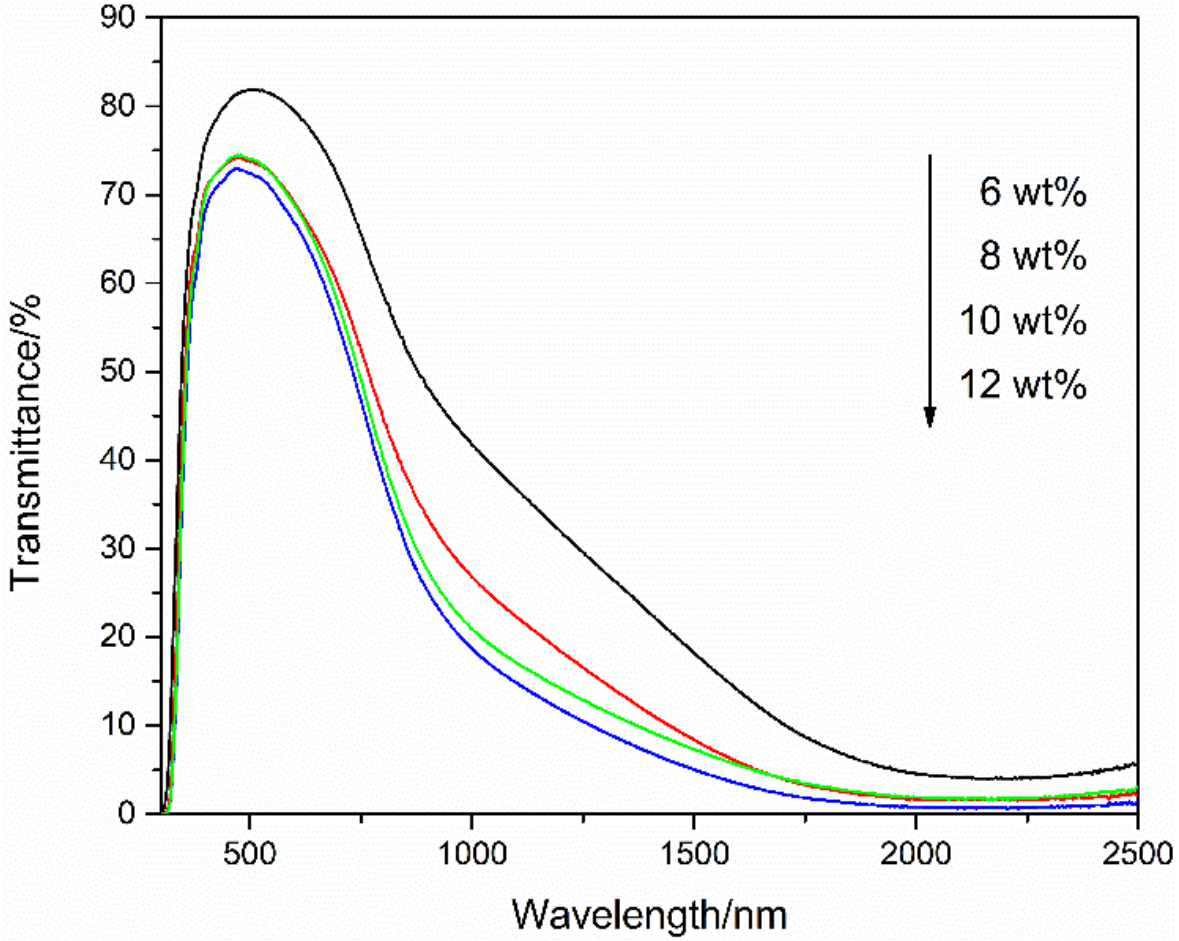

Fig. 6 UV-Vis-NIR transmittance spectra of spectrally selective coatings prepared by dispersions with different solid content of the composite nanofiller

Figure 7

Click here to download Figure: Fig. 7.docx

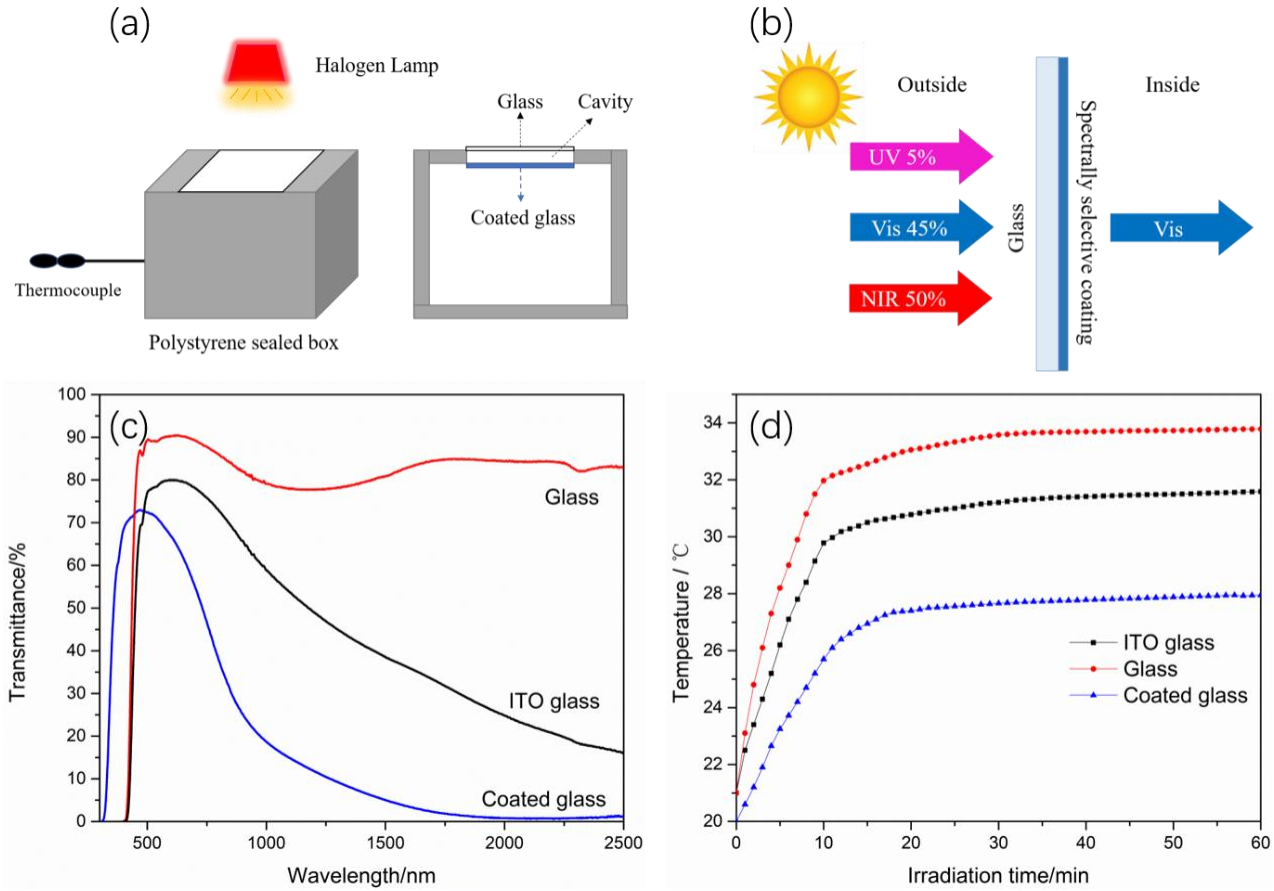

Fig. 7 (a) Schematic of the device for near-infrared shielding test, (b) Diagram of the transparent heat-shielding mechanism for the coated glass, (c) The UV-Vis-NIR transmittance spectra of coated glass, ITO glass and ordinary glass and (d) The temperature variation of three glass samples with the irradiation time